SAE INTERNATIONAL

ARTICLE INFO
Article ID: 03-15-03-0022

doi:10.4271/03-15-03-0022

Numerical Assessment of Additive Manufacturing-Enabled Innovative Piston Bowl Design for a Light-Duty Diesel Engine Achieving Ultra-Low Engine-Out Soot Emissions

Federico Millo,[1] Andrea Piano,[1] Salvatore Roggio,[1] Andrea Bianco,[2] Francesco Concetto Pesce,[3] and Alberto Lorenzo Vassallo[3]

[1]Politecnico di Torino, Italy
[2]Powertech Engineering, Italy
[3]PUNCH Torino S.p.A/ formerly General Motors Global Propulsion Systems, Italy

Abstract

The design of diesel engine piston bowls plays a fundamental role in the optimization of the combustion process, to achieve ultra-low soot emissions. With this aim, an innovative piston bowl design for a 1.6-liter light-duty diesel engine was developed through a steel-based additive manufacturing (AM) technique, featuring both a sharp step and radial bumps in the inner bowl rim. The potential benefits of the proposed hybrid bowl were assessed through a validated three-dimensional computational fluid dynamics (3D-CFD) model, including a calibrated spray model and detailed chemistry. Firstly, the optimal spray targeting was identified for the novel hybrid bowl over different injector protrusions and two swirl ratio (SR) levels. Considering the optimal spray targeting, an analysis of the combustion process was carried out over different engine working points, both in terms of flame-wall interaction and soot formation. At rated power engine operating conditions, the hybrid bowl highlighted faster mixing-controlled combustion due to the reduced flame-to-flame interaction and the higher air entrainment into the flame front. At partial-load operating points, the hybrid bowl showed a remarkable soot reduction in comparison with the re-entrant bowl due to a more intense soot oxidation rate in the late combustion phase. Moreover, for the hybrid bowl, a robust Exhaust Gas Recirculation (EGR) tolerance was highlighted, leading to a flat soot-brake-specific oxides of nitrogen ($BSNO_x$) trade-off. At constant $BSNO_x$, a 70% soot reduction was achieved without any detrimental effect on fuel consumption, suggesting the high potential of the proposed innovative bowl for soot attenuation.

History

Received: 02 Jul 2021
Revised: 03 Sep 2021
Accepted: 17 Sep 2021
e-Available: 28 Sep 2021

Keywords

Diesel engine, Piston geometry, Numerical simulation, Spray-wall interaction

Citation

Millo, F., Piano, A., Roggio, S., Bianco, A. et al., "Numerical Assessment of Additive Manufacturing-Enabled Innovative Piston Bowl Design for a Light-Duty Diesel Engine Achieving Ultra-Low Engine-Out Soot Emissions," *SAE Int. J. Engines* 15(3):2022, doi:10.4271/03-15-03-0022.

ISSN: 1946-3936
e-ISSN: 1946-3944

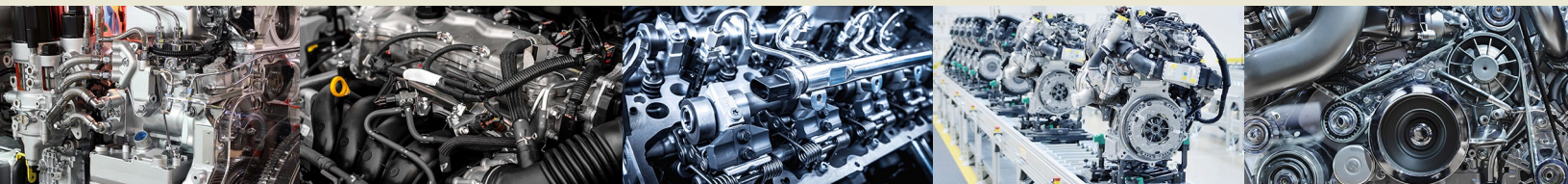

1. Introduction

Nowadays, the transportation sector is facing more demanding carbon dioxide (CO_2) legislative targets and tighter emissions regulations. The need to comply with the new standards is pushing the OEMs toward the exploitation of innovative technologies for cleaner combustion systems. Regarding diesel engines, several solutions have been investigated to improve the soot-nitrogen oxides (NO_x) trade-off, such as new combustion modes [1, 2] or the use of alternative fuels [3, 4]. Moreover, aftertreatment systems such as Selective Catalytic Reduction (SCR) have shown the capability to respect even the NO_x limits under real-driving conditions without any remarkable fuel consumption drawbacks [5]. However, the significant production cost could dramatically affect the future diesel market penetration [6]. Therefore, the in-cylinder control of pollutant emissions will still play a fundamental role to reach the regulations while limiting the engine cost [7, 8]. In this scenario, great attention has been paid to the piston bowl optimization since the improved flame-to-wall interaction was found to be crucial for higher engine efficiency and lower pollutant emissions [9].

In the last years, one of the main alternatives to the conventional re-entrant bowl for a light-duty diesel engine was represented by the stepped-lip bowl [10]. This bowl geometry is characterized by the presence of a chamfered lip instead of the protruding lip used for a re-entrant bowl. Directing the injected fuel to the chamfered lip, the stepped-lip bowl can create two counterrotating toroidal vortices, inward within the bowl and outward in the head/squish region, enhancing the air/fuel mixing [11]. Thanks to the improved mixing, the stepped-lip bowl highlighted high tolerance to the Exhaust Gas Recirculation (EGR), which can be adopted for NO_x control in combination with higher injection pressure for soot reduction [12]. Moreover, this concept had shown high potential to reach the emissions limits even without any aftertreatment system, as stated by Cornwell and Smith in [13, 14] for a JCCB off-highway diesel engine. Recently, a stepped-lip design was implemented in the Mercedes-Benz OM 654 engine, showing improved engine efficiency and soot reduction [15]. Nevertheless, the beneficial flow structures provided by this concept are strictly related to the spray targeting optimization, as numerically evaluated in [11]. The flow structures investigation, thanks to the Combustion Image Velocimetry (CIV), highlighted a strong correlation between the formation of long-lasting toroidal vortices due to the stepped lip and the enhanced burn rate in the late combustion [16]. However, only for a limited range of injection timing, a faster Heat Release Rate (HRR) in the late combustion phase can be observed, as shown by Bush et al. in [17]. Another benefit provided by the stepped-lip bowl is the reduced heat transfer losses due to the lower bowl surface and the reduced flame propagation toward the liner [18]. The fuel split on the step and the formation of dual vortices provides a more even air/fuel mixing process, fundamental to improve the soot oxidation rate in the late combustion phase [19], as also numerically evaluated in [20].

For low-swirl heavy-duty engines, which typically involve an open bowl shape [21], the flame-to-flame interaction results in a lower combustion rate and higher soot formation [22]. To overcome this phenomenon, Volvo patented in 2013 the wave-shaped bowl [23], adding radial protrusions in the regions where two adjacent flames usually collide. This combustion system can enhance the late-cycle mixing, as investigated through numerical and optical techniques by Eismark et al. in [24]. The radial bumps lead to a different collision angle between adjacent flames, mitigating the formation of rich stagnation zones and increasing the flame velocity toward the cylinder center [24]. Therefore, a more intense Radial Mixing Zone (RMZ) is formed, which results in higher air mixing into the leading edge of the flame [24]. Moving ahead in the combustion process, when the RMZ detaches from the wall, the trailing edge of the flame highlights more intense air entrainment, resulting in a faster burn rate [24]. This enhanced mixing mechanism leads to a higher HRR in the mixing-controlled combustion phase in comparison with a conventional bowl, and up to 1% thermal efficiency increment can be gained, as assessed by Zhang et al. in [4]. The wave bowl effects on the late-cycle soot oxidation rate are even more relevant. Single-Cylinder Engine (SCE) tests over different partial-load engine operating conditions have shown an impressive improvement on soot-NO_x trade-off, reaching up to 80% soot reduction for the wave bowl [24]. Combining the improved mixing mechanism for the wave bowl with an oxygenated fuel, a further soot reduction can be obtained, limiting NO_x with a higher EGR rate [25]. Although the wave concept has shown high potential for reducing both fuel consumption and soot emissions for a heavy-duty engine, further analyses are required to understand its impact on combustion evolution for a light-duty engine. In this case, the higher SR could reduce the RMZ propagation, while the usual re-entrant design could cause a higher flame recirculation toward the piston dome (tumbling vortex). Recently, the potential benefits of including radial bumps in a light-duty diesel engine was numerically evaluated [26]. In this work, the radial-bumps bowl highlighted a higher air/fuel mixing rate with respect to a conventional re-entrant bowl. At partial-load engine operating conditions, a flatness in the trade-off over an EGR sweep was observed, providing a 50% soot reduction and 5% Brake-Specific Fuel Consumption (BSFC) improvement than with the re-entrant bowl [26].

In the last years, the introduction of Additive Manufacturing (AM) techniques has allowed to exploit the potential of high complexity and undercut geometries for further optimization of the piston bowl design [27, 28]. In this context, the potential of a synergy between the stepped-lip and radial-bumps bowls, enabled by a steel-based AM technique, was investigated by Belgiorno et al. in [28]. In this work, an innovative piston bowl design was presented, featuring both a highly re-entrant sharp-stepped bowl and a number of radial bumps equal to the nozzle holes in the inner bowl rim. SCE tests highlighted for this concept an impressive soot reduction with any detrimental effects on fuel consumption [28]. The impact of a similar concept on the combustion

evolution was carried out through a single-cylinder optical access engine campaign by Pastor et al. in [29, 30]. Introducing radial bumps leads to higher flame reverse flow and faster late-cycle oxidation in comparison with the re-entrant bowl [29]. Moreover, a higher soot oxidation rate in the late combustion phase was observed, at different engine loads, fuel injection parameters, and EGR rates [30].

Considering the previously mentioned benefits provided by the optimization of the piston bowl design, this work aims to assess the potential of a novel piston bowl geometry for a light-duty diesel engine. In a similar way to the piston bowl proposed in [28], it combines two crucial features as a stepped lip and radial protrusions, aiming for higher engine efficiency and lower soot emissions. The impact of this innovative piston bowl on the combustion process was carried out through Computational Fluid Dynamics (CFD) simulations. The simulation methodology was based on an integrated and automated one-dimensional/three-dimensional (1D-/3D-) CFD coupling methodology, which was widely reported in [31]. The 1D-CFD models [32, 33, 34] provided the time-dependent boundary conditions and a reliable injection rate profile, while the in-cylinder combustion evolution was investigated through 3D-CFD simulations. In the first part of the work, the spray targeting was optimized over different injector protrusions and two SR levels. Then the optimal calibration was widely investigated in terms of near-wall flame evolution and soot formation/oxidation process for three different engine operating conditions: one at rated power and two at partial load. Finally, an EGR rate sweep was carried out under partial-load operating conditions to understand the combustion system's performance in terms of fuel consumption reduction and pollutant emissions' formation mitigation.

2. Case Study

2.1. Test Engine

The numerical analysis was carried out having as a case study, a diesel engine developed for passenger car applications whose main characteristics are listed in Table 1. It is a four-cylinder turbocharged compression ignition engine and features a state-of-the-art common rail fuel injection system with the latest generation eight-hole solenoid injector able to reach a maximum rail pressure of 2000 bar.

TABLE 1 Test engine main features.

Cylinders #	4
Displacement	1.6 L
Bore × Stroke	79.7 mm × 80.1 mm
Compression ratio	16:1
Turbocharger	Single-stage with variable geometry turbine (VGT)
Fuel injection system	Common rail Max rail pressure 2000 bar
Maximum power	100 kW at 4000 RPM
Maximum torque	320 Nm at 2000 RPM

FIGURE 1 Piston bowl geometries under investigation. Left: re-entrant; right: hybrid.

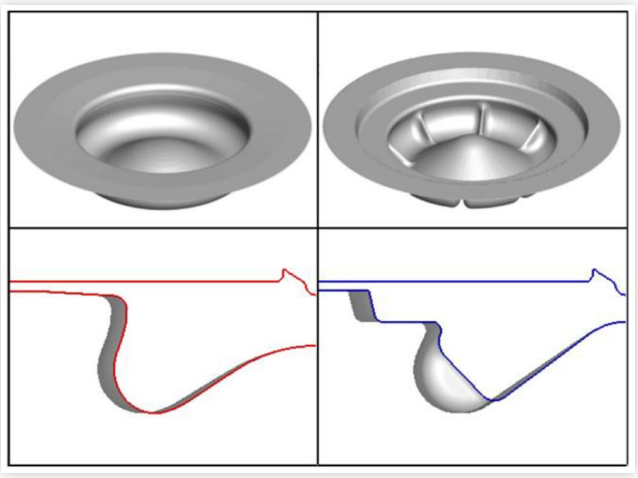

To assess the potential of the new innovative bowl, it has been compared with the baseline combustion system, a conventional re-entrant bowl design, as shown in Figure 1, left. On the other side, the innovative piston bowl (hereinafter named as "hybrid") features an annular step and a number of radial bumps in the inner bowl rim equal to the injector nozzle holes, as shown in Figure 1, right. For this latter bowl design, a reduced compression ratio (i.e., 15:1) was considered keeping the bore and squish height equal to the ones of the re-entrant design. As widely investigated in [28], a steel-based AM technique was selected to build up the hybrid bowl due to the high level of geometrical complexity and the durability needs for a diesel engine application. The lattice structure of the oil gallery, designed as an open-cell frame, provided the best results in terms of oil recirculation and lightweighting [28]. Moreover, thanks to AM approach, the inner area of the piston was topologically optimized [28].

Three different engine working points (WP), reported in Table 2, were selected for the analysis: two partial-loads operating conditions (WP1, WP2) were considered since they are representative of a typical type-approval driving cycle engine conditions, while WP3 was analyzed to evaluate the proposed innovative bowl design at rated power.

TABLE 2 Selected engine working points.

	Speed [RPM]	BMEP [bar]
WP1	1500	5.0
WP2	2000	8.0
WP3	4000	18.5

2.2. Simulation Setup

The simulation methodology was based on a previously developed and validated 1D-/3D-CFD codes coupling, widely described in [31]. The 1D-CFD complete engine model, built in GT-SUITE and validated in [32], provided the time-dependent boundary conditions (pressure, temperature, and species concentration) at the intake and exhaust ports for the first step of the multidimensional simulation, named "cold flow." This analysis, performed in CONVERGE CFD, was used to analyze both the in-cylinder flow field and the thermodynamic conditions during the gas exchange process. Then, starting from the Intake Valve Closure (IVC), the compression stroke and the combustion processes were simulated considering only a single sector of the full-cylinder geometry centered along a single spray axis. The injection rate profile was provided by a previously developed 1D-CFD injector model [33, 34], which requires as inputs the rail pressure and the energizing and dwell times. In the last step of the methodology, the 3D-CFD combustion results were post-processed in a GT-SUITE environment to guarantee the same solution methodology of the initial 1D-CFD complete engine model.

Regarding 3D-CFD combustion simulation, a base grid size of 0.50 mm for all directions was selected, while a minimum grid size of 0.25 mm was considered. Indeed, thanks to permanent Adaptive Mesh Refinement (AMR), an additional grid refinement was considered, depending on the curvature (second derivative) in specific field variables (i.e., velocity and temperature) [35]. In addition, a single level of fixed embedding technique was set for the injector cone angle to properly resolve the fuel spray. For spatial discretization, a second-order central difference scheme was adopted, while, for temporal discretization, a first-order implicit Euler scheme was considered to maintain stability. The conservation equations were solved through the PISO (Pressure-Implicit with Splitting of Operators) algorithm of Issa [36] and the Rhie-Chow scheme for pressure-velocity coupling [37]. As far as turbulence modeling is concerned, the Reynolds-averaged Navier-Stokes (RANS)-based Renormalization Group (RNG) k-ε model [38] was adopted, thus guaranteeing the effects of flame-induced compression, expansion, and rapid strain on the turbulent quantities [39]. The law-of-walls approach with standard wall functions was used for the kinematic and thermal description of the boundary layers [40]. Moreover, the turbulent heat transfer was modeled utilizing the O'Rourke and Amsden model [41].

The spray model was based on the "blob" injection method [42], and the breakup of droplets was modeled using a calibrated Kelvin-Helmholtz and Rayleigh-Taylor (KH-RT) model [42]. An overview of the spray submodels adopted in the simulation setup is reported in Table 3.

The SAGE detailed chemistry was adopted as a combustion model, featuring the Skeletal Zeuch reaction mechanism for N-Heptane oxidation (121 species, 593 reactions) [47]. This reaction scheme implements the Polycyclic Aromatic Hydrocarbons (PAH) soot precursor chemistry, thus enabling the Particulate Mimic (PM) soot model for the in-cylinder soot mass prediction [48, 49, 50], while the NO_x reactions are embedded in the chemistry scheme.

TABLE 3 Spray submodels.

Discharge coefficient model	Cv correlation [35]
Breakup model	Calibrated KH-RT
Turbulent dispersion	O'Rourke model [43]
Collision model	No Time Counter (NTC) collision [44]
Drop drag model	Dynamic drop drag [45]
Evaporation model	Frossling model [43]
Wall film model	O'Rourke [46]

3. Numerical Analysis

3.1. Spray Targeting Optimization

To properly evaluate the potential of the innovative piston bowl design, the spray targeting optimization was performed by changing the injector protrusion to minimize both the engine-out soot emissions and fuel consumption. NO_x emissions were not considered at this stage since the expected low-soot potential could increase the EGR tolerance, thus keeping the NO_x level under control. Therefore, the same engine calibration of the baseline re-entrant bowl in terms of boost pressure, EGR rate, and injection parameters was considered. In addition, two different SR levels were tested (i.e., baseline and half) to identify the best coupling among the swirling flow and the flow structures induced by the radial bumps. As depicted in Figure 2, four injector protrusions were tested: the nominal protrusion, equal to the one adopted in the baseline combustion system (0) and 1 mm and 2 mm below (−1, −2, respectively) and 1mm above (+1) the nominal position. The spray targeting optimization was carried out at rated power condition (WP3 in Table 2), and the optimal configuration was then validated at partial load (WP1).

Soot-Brake-Specific NO_x ($BSNO_x$) and BSFC-$BSNO_x$ trade-offs for the WP3 are depicted in Figure 3, top and bottom, respectively. The results were normalized with respect

FIGURE 2 Injector protrusions for spray targeting optimization.

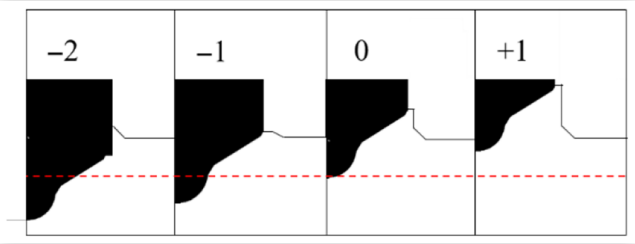

FIGURE 3 Injector protrusion sensitivity for two SR levels: normalized trade-offs with respect to the baseline configuration. Top: soot-BSNO$_x$ trade-off; bottom: BSFC-BSNO$_x$ trade-off. WP3: 4000 RPM × 18.5 bar BMEP.

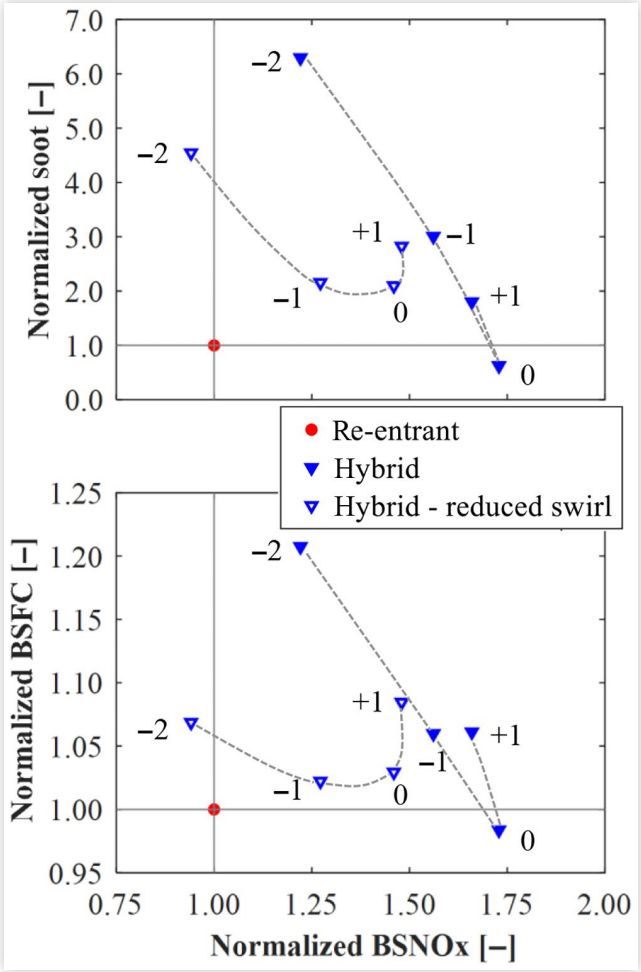

to the baseline engine configuration (i.e., re-entrant bowl, nominal injector protrusion, nominal SR). At nominal SR, the hybrid bowl highlights a remarkable sensitivity to the injector protrusion especially in the soot-BSNO$_x$ trade-off: adopting the nominal protrusion, the hybrid bowl provides the highest soot reduction (−40% in comparison with the re-entrant bowl), while moving to different injector protrusions results in higher soot. More specifically, not only when the injector protrusion is equal to +1 mm (+1) but also considering a more protrusive injector tip (−2, −1), at constant start of the main injection, the fuel split on the step becomes unbalanced, significantly increasing the soot formation up to six times higher soot in comparison with the re-entrant bowl. The unbalanced fuel split has a noticeable influence on the mixing-controlled combustion, leading to an engine efficiency worsening. The optimal configuration is provided by the nominal injector protrusion (0), thanks to which a 2% reduction in BSFC with respect to the re-entrant bowl is achieved. Moreover, in halving the SR, the trade-off results are noticeably affected with an overall reduction of both the NO$_x$ emissions and soot-BSFC sensitivity. Also, in this case, the nominal configuration has provided the best results among the different injector protrusions; however, if compared with the baseline re-entrant combustion system, two times higher soot and +3% higher BSFC were obtained. Therefore, even considering the strong interaction between the radial bumps and the swirling flow [26], the hybrid bowl requires higher SR to increase the air/fuel mixing rate for a more efficient combustion process.

To further understand the injector protrusion sensitivity upon the combustion process, a fuel-rich mass index was defined as the cylinder mass with an equivalence ratio higher than 1.5 divided by the entire cylinder mass, following Equation 1. In this way, this cylinder rich mass fraction provides an index of the soot emission formation due to the rich mixture combustion.

$$\text{Cylinder rich mass fraction} = \frac{\text{Cylinder mass}_{\text{equiv ratio}>1.5}}{\text{Cylinder mass}} \quad \text{Eq. (1)}$$

This index was computed considering both the whole combustion chamber and a reduced cylinder domain as the volume below the horizontal plane cutting the step at TDC. Thanks to the latter, quantitative information concerning the fuel split and its impact on the combustion and emissions formation processes can be detected. The results of the analysis were reported in Figure 5 for the three different crank angle degrees (CAD) during the injection event shown in Figure 4.

At the top dead center (TDC) [Figure 5(a)], the total cylinder rich mass is comparable over the different injector protrusions, suggesting a similar air/fuel mixing rate although the different fuels split on the step. Indeed, focusing on the cylinder rich mass below the step, a significant variation can be observed among the injector protrusions, moving from almost 100% (injector protrusion, −2) to 20% (injector protrusion, +1) of the total cylinder rich mass. As highlighted in Figure 3, the best results both in terms of soot and BSFC were obtained with the nominal injector protrusion, where the optimal fuel split (50% of the total cylinder rich mass is below

FIGURE 4 Injection rate profile and CAD for injector protrusion sensitivity. WP3: 4000 RPM × 18.5 bar BMEP.

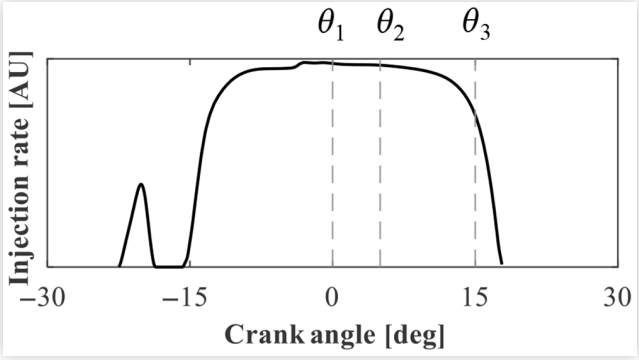

FIGURE 5 Cylinder rich mass fraction (equivalence ratio higher than 1.5) for the whole combustion chamber (total) and below the horizontal plane cutting the step at TDC (below the step). WP3: 4000 RPM × 18.5 bar BMEP.

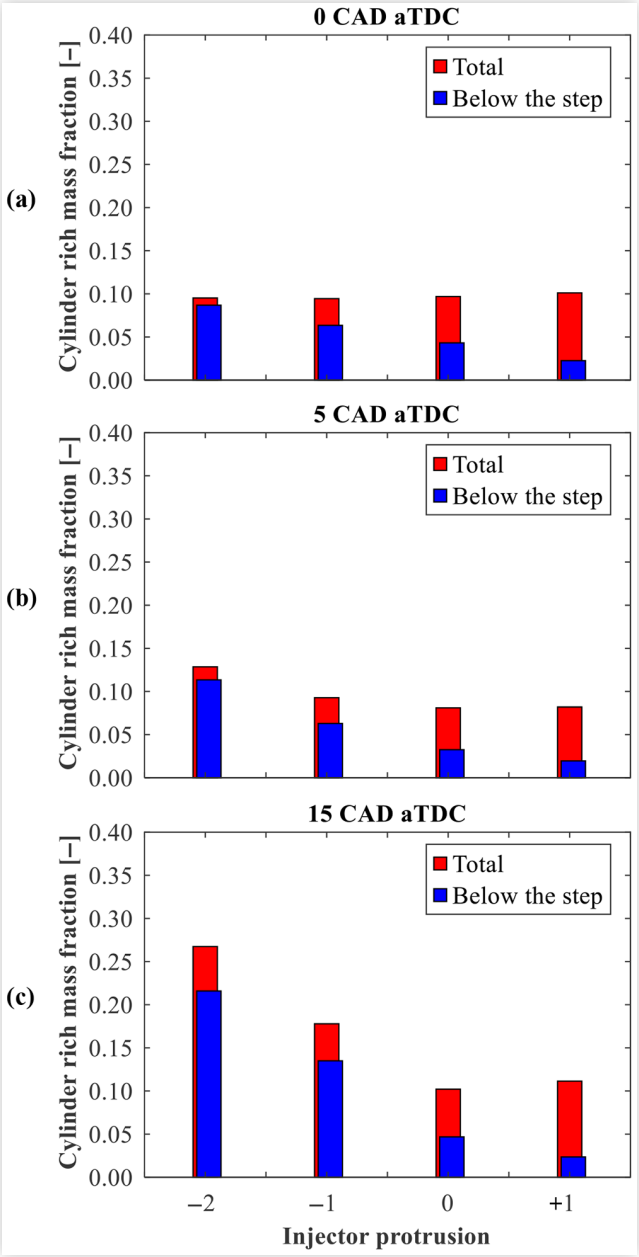

the step) can be observed. Moving ahead in the injection event, at +5 CAD aTDC, the injection protrusions −2 and −1 show higher cylinder rich mass, mainly placed below the step. This unbalanced fuel split above and below the step, on one hand, creates a rich distribution within the bowl, thus promoting soot formation and, on the other hand, reduces the air utilization in the squish region, decreasing the combustion rate. The lowest injector protrusion (+1), even without optimal fuel split, shows a total cylinder rich mass comparable with the nominal injector protrusion, suggesting a similar oxidation rate. Close to the End of Injection (EOI), at +15 CAD aTDC, differences among the tested injector protrusions become more evident. The −2 and −1 injector protrusions show a dramatic increment of the cylinder rich mass leading to higher soot formation below the step, as already highlighted in Figure 3. Moreover, the higher residual fuel, especially below the step, extends the combustion duration leading to higher BSFC than with the nominal protrusion. Reducing the injector protrusion (+1), the total cylinder rich mass rises over the value obtained for the nominal injector protrusion and the fuel split results unbalanced between the abovementioned cylinder domains (total cylinder and below the step volumes). Indeed, the higher fuel concentration above the step can be slowly and not efficiently oxidized, leading to a higher soot content and longer combustion duration.

To better highlight the fuel split on the step, assessing the spray-wall interaction and its effect on flame evolution, the equivalence ratio distribution during the injection event (at the three different CAD already showed in Figure 4) was analyzed in Figure 6. This latter shows, for each injector protrusion under investigation, the equivalence ratio contour plot on a vertical plane including the cylinder and spray axes, and the isoline at a constant temperature equal to 1500 K (black line), which was selected as representative of the flame front. At TDC [Figure 6(a)], the flame front with the most protrusive injector tip (−2) mainly propagates toward the cylinder axis due to the spray targeting below the step, increasing the air entrainment, thanks to the higher oxygen content placed near the cylinder axis. Decreasing the injector protrusion results in higher flame redistribution above the step and thereby in higher air utilization in the squish region. Therefore, at this stage, although the different fuels split by varying the injector protrusion, similar air utilization is observed pushing the flame toward the cylinder center or in the squish region, confirming the trends highlighted in Figure 5(a). The differences among the injector protrusions become more evident at +5 CAD aTDC [Figure 6(b)]. Adopting the −2, −1 injector protrusion results in poor air utilization in the squish region, as highlighted by the unbalanced split in Figure 5(b). The oxygen content in the dome region is significantly reduced due to the faster flame recirculation toward the piston center (reverse flow). In addition, the flame reverse flow strongly interacts with the spray core, further increasing the cylinder rich mass. The nominal injector protrusion leads to a balanced fuel split on the step, optimizing the air utilization inward within the bowl volume and upward above the step. Moreover, the interaction between the reverse flow and the spray core is avoided. Reducing the injector protrusion (+1), the flame is pushed upward above the step where higher air utilization can be observed while reducing the oxidation process within the bowl in comparison with the nominal protrusion. Moving toward the EOI, at +15 CAD aTDC, the highest injector protrusions (−2, −1) show a higher rich mass within the bowl than with the nominal protrusion, dramatically increasing the soot formation in the piston dome, without using the

FIGURE 6 Equivalence ratio contour plot on the selected vertical plane, for each injector protrusion under investigation with nominal SR. Black line: isoline at a constant temperature equal to 1500 K. WP3: 4000 RPM × 18.5 bar BMEP.

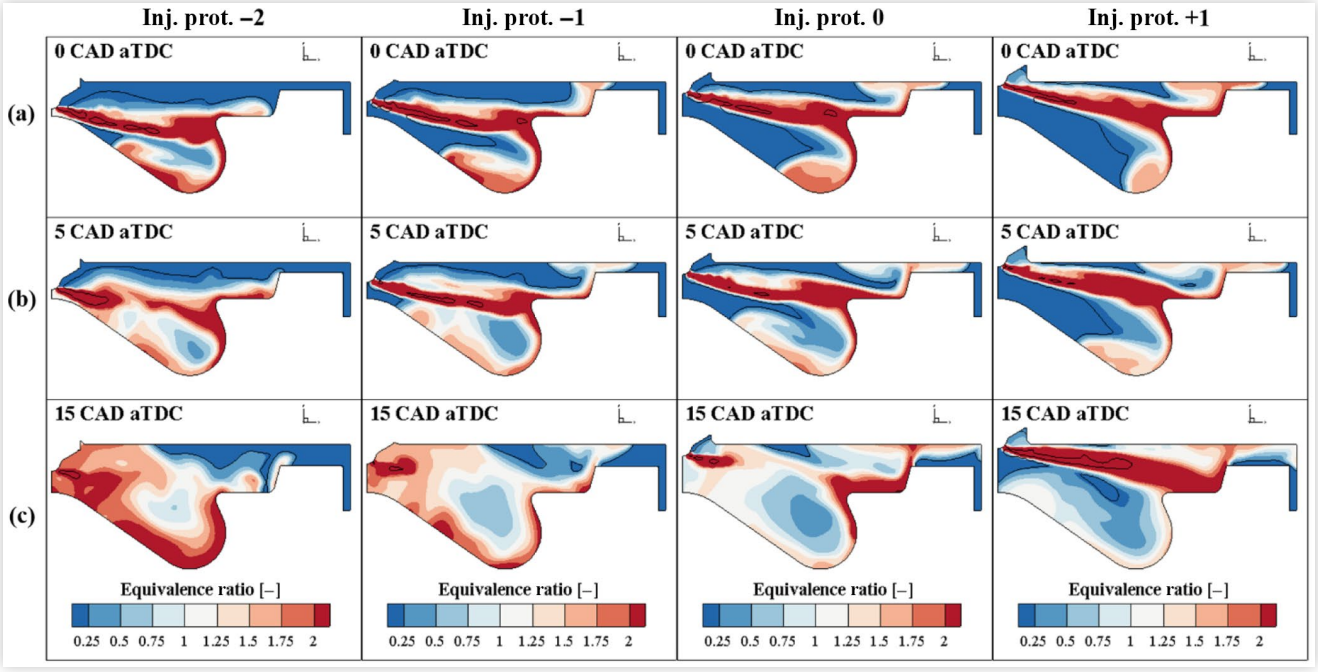

available oxygen content in the squish region. On the other side, reducing the injector protrusion, the fuel jet is mainly directed above the step toward the cylinder head where the absence of available oxygen could result in a higher soot formation.

To further understand the effect of different SRs on the combustion process, as already shown in Figure 3, the equivalence ratio distribution for the nominal injector protrusion at +15 CAD aTDC was analyzed and is reported in Figure 7.

FIGURE 7 Equivalence ratio bins distribution for the nominal injector protrusion at +15 CAD aTDC. WP3: 4000 RPM × 18.5 bar BMEP.

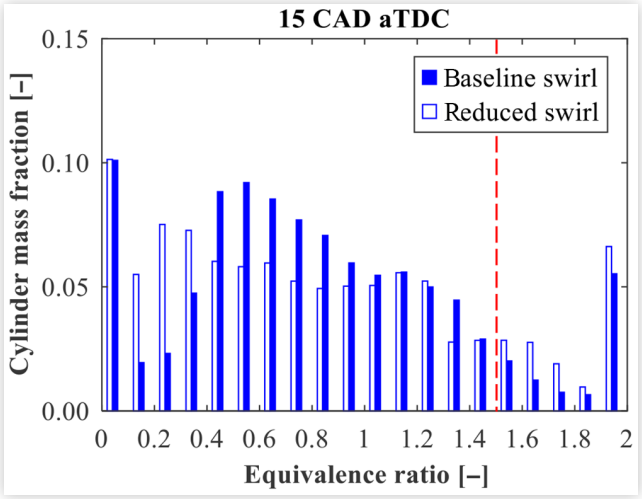

The total cylinder mass was binned by equivalence ratio into twenty intervals, starting from 0÷0.1 bin that corresponds to pure ambient gas, for both the baseline and the reduced SR. Differently from the latter, the nominal SR shows the mode of the distribution closer to the stoichiometric range, while a reduced cylinder mass fraction can be observed in the tails of the distribution (0.1÷0.4 and 1.5÷2 equivalence ratio bins). Therefore, the distribution obtained with the baseline SR suggests a faster and more efficient combustion process, and lower soot, thanks to the reduced cylinder mass fraction at a high equivalence ratio, thus confirming the trade-off results in Figure 3. The red dashed line in Figure 7 represents an equivalence ratio equal to 1.5, already selected in Equation 1 as a tracer for the cylinder rich mass fraction. The reduced swirl highlights a higher cylinder mass fraction in the 1.5÷2 equivalence ratio bins, thus being more prone to soot formation.

Extending the analysis at partial-load engine operating conditions (WP1), similar trends were obtained, as shown in Figure 8. In this case, once the benefit of more intense swirling flow at rated power was assessed, only the baseline SR was considered. Also at partial load, the hybrid bowl with the nominal protrusion provides a noticeable soot reduction (−70%) than with the re-entrant bowl, coupled with a slight improvement of BSFC (lower than 1%).

The spray targeting optimization has identified the best solution both for partial- and full-load engine operating conditions. Therefore, unless otherwise noted, in the following analysis, the hybrid bowl will feature nominal injector protrusion and SR.

FIGURE 8 Injector protrusion sensitivity for the nominal SR: normalized trade-offs with respect to the baseline configuration. Top: soot-BSNO$_x$ trade-off; bottom: BSFC-BSNO$_x$ trade-off. WP1: 1500 RPM × 5.0 bar BMEP.

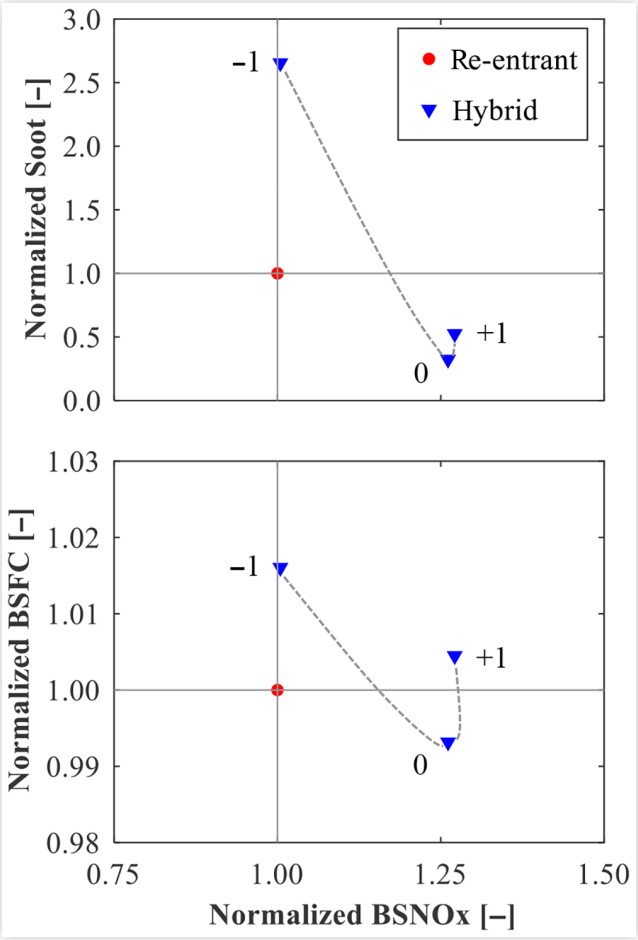

FIGURE 9 HRR and injection rate profile. WP3: 4000 RPM × 18.5 bar BMEP.

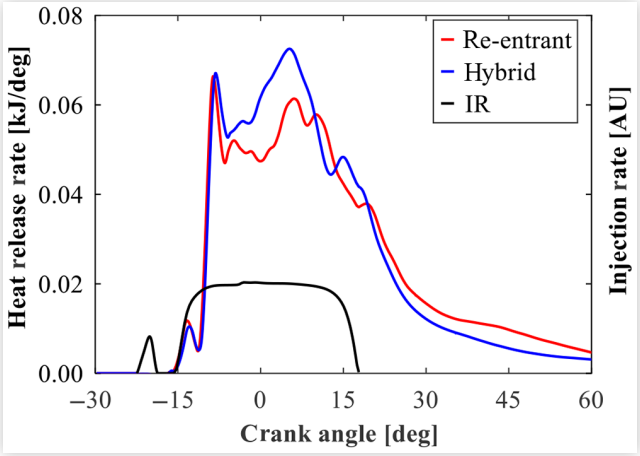

3.2. Combustion Analysis

Full-Load Engine Operating Condition (WP3) Once the optimal configuration in terms of injection protrusion and SR was assessed, the combustion systems' effects on the combustion development were investigated. To do this, the HRR and the injection rate profile for each combustion system are depicted in Figure 9. During the free spray development (from −20 CAD to −5 CAD aTDC), the piston bowl geometry slightly affects the combustion process and comparable HRR can be observed for both the combustion systems. Moving toward the TDC, the hybrid bowl shows a higher HRR in comparison with the re-entrant bowl, but they become again similar close to the EOI. At this stage, the high fuel concentration above the step reduces the air utilization within the bowl. Moving ahead in the cycle, after the EOI, the re-entrant bowl highlights a higher HRR than with the hybrid bowl due to the higher residual fuel to be burned.

To further understand the near-wall flame development, the equivalence ratio distribution was investigated during the main injection event and is shown in Figure 10 for both the baseline re-entrant and the innovative hybrid bowls. Three horizontal planes, parallel to the cylinder head, were selected to represent the numerical results. Referring to the hybrid bowl, the plane Z1 corresponds to the step, while the planes Z2 and plane Z3 are in the radial bump region (low curvature, low depth upper-bump and high curvature, and high depth bottom-bump regions, respectively). Moreover, a two-sector representation was chosen to better identify the flame evolution of two adjacent jets on the radial bump region. Considering the step region [Figure 10(a)], the re-entrant bowl shows a stronger flame-to-flame interaction, leading to a higher loss of kinetics, as also stated in [24]. On the contrary, the hybrid bowl mitigates the collision of adjacent flames since the fuel jet momentum redistribution above and below the step reduces the tangential velocity of the flame over the bowl surface. In the upper-bump region [Figure 10(b)], the radial bumps dramatically affect the flame evolution: they simultaneously minimize the flame-to-flame interaction and drives the flame front toward the cylinder axis and downward the bump tip into the consecutive sector where high oxygen concentration is present, as shown by the black dashed arrow. Therefore, higher air entrainment onto the flame front can be expected, thus increasing the combustion rate as highlighted in the HRR in Figure 9. Moving to the bottom-bump region [Figure 10(c)], the differences between the combustion systems become even more evident. Indeed the re-entrant bowl highlights a strong interaction between the adjacent flames, resulting in a single merged flame front, thus limiting the oxidation rate and fostering the soot emission formation.

FIGURE 10 Equivalence ratio contour plot at TDC on the selected cutting planes Z1 (a), Z2 (b), and Z3 (c). Black line: isoline at a constant temperature equal to 1500 K. Left: re-entrant; right: hybrid. WP3: 4000 RPM × 18.5 bar BMEP.

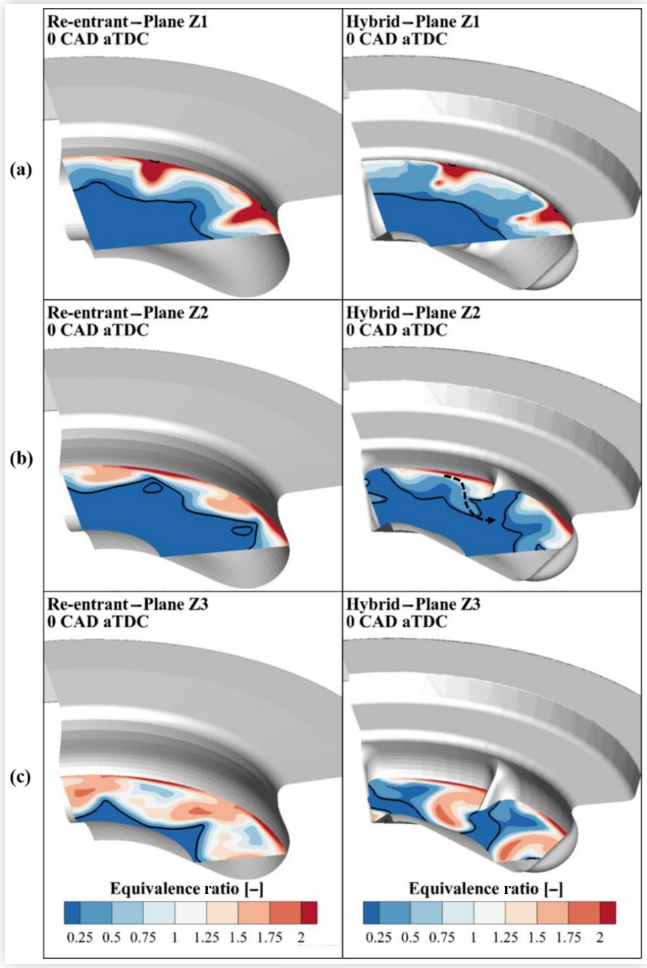

Instead, the hybrid bowl avoids the flames collision, thanks to the bottom-bump geometry, where each flame front appears well separated by the radial bumps. Therefore, the surrounding oxygen can be efficiently mixed, resulting in a faster combustion process.

Partial-Load Engine Operating Condition (WP1) The beneficial effects on the combustion process thanks to the hybrid bowl were also investigated under partial-load operating conditions, 1500 RPM × 5.0 bar BMEP (WP1 in Table 2). The results in terms of HRR for each combustion system under investigation are shown in Figure 11. The re-entrant bowl highlights a higher premixed main combustion phase near the TDC. Indeed the higher SR obtained with the baseline re-entrant bowl [26] impacts the spray

FIGURE 11 HRR and injection rate profile. WP1: 1500 RPM × 5.0 bar BMEP.

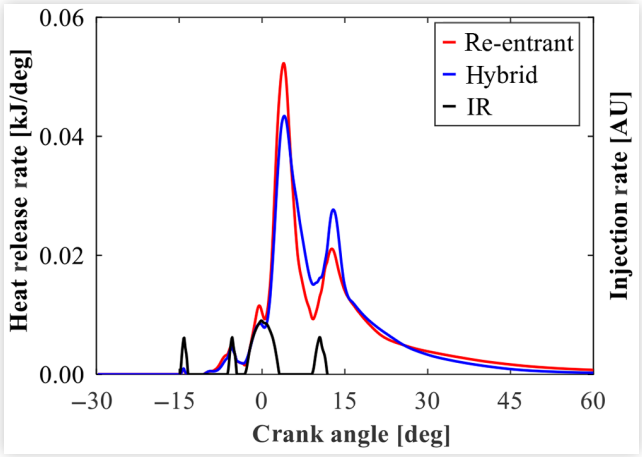

development, reducing the flame impingement on the bowl surface and increasing the air-fuel mixing. This results in a lower loss of kinetics, increasing the combustion rate, as also stated in [24]. Nevertheless, after the main EOI, when the flame-to-flame interaction affects the combustion of the re-entrant design reducing the combustion rate, the hybrid bowl minimizes this counterproductive effect and the HRR rises over than with the re-entrant bowl. This becomes even more evident during the after-injection burn-out when the hybrid bowl continues to show higher HRR, thanks to the fuel split on the step that increases the fuel concentration in the squish area enhancing the air utilization, as also reported by Dolak et al. in [51].

To further understand the piston bowl geometry effects on the combustion process, the equivalence ratio distribution was investigated. Figure 12 shows the equivalence ratio contour plot at +10 CAD aTDC on the same cutting planes highlighted in Figure 10. Considering the step region [Figure 12(a)], as also assessed for WP3, the hybrid design evinces reduced tangential velocity over the bowl surface and provides lower flames interaction. Moreover, the higher dome curvature increases the upward velocity of the tumbling vortex induced by the reverse flow. Indeed the flame is moved toward the cylinder head, as highlighted by the flame cloud close to the center of the bowl. In the upper-bump region [Figure 12(b)], the re-entrant bowl shows an intense flames collision area near the bowl surface. The resulting rich pockets dramatically reduce the oxidation rate onto the flame front and high soot emission is expected. On the contrary, the radial bumps of the hybrid bowl are effective in reducing the flame-to-flame interaction and in moving the fuel toward the cylinder axis enhancing the so-called RMZ, beneficial for soot emissions and efficiency. The advanced flame toward the piston dome is driven by the reverse flow that becomes more intense since the radial bumps break the macro swirling flow, as also

FIGURE 12 Equivalence ratio contour plot at +10 CAD aTDC on the selected cutting planes Z1 (a), Z2 (b), and Z3 (c). Black line: isoline at a constant temperature equal to 1500 K. Left: re-entrant; right: hybrid. WP1: 1500 RPM × 5.0 bar BMEP.

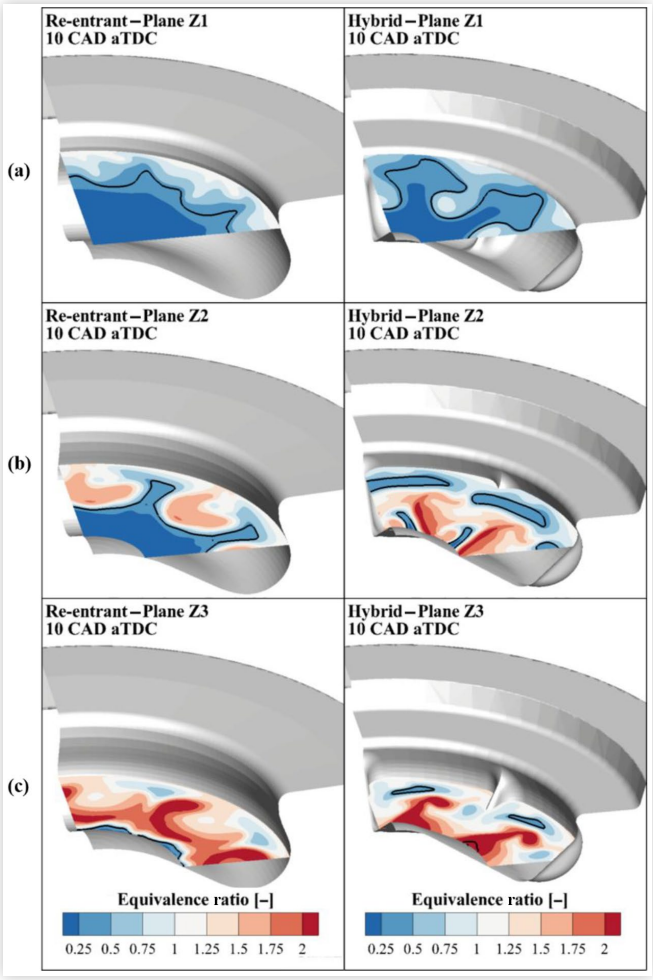

FIGURE 13 Soot PM model results. Top: in-cylinder soot mass; bottom: net formation rate of in-cylinder soot mass. WP1: 1500 RPM × 5.0 bar BMEP.

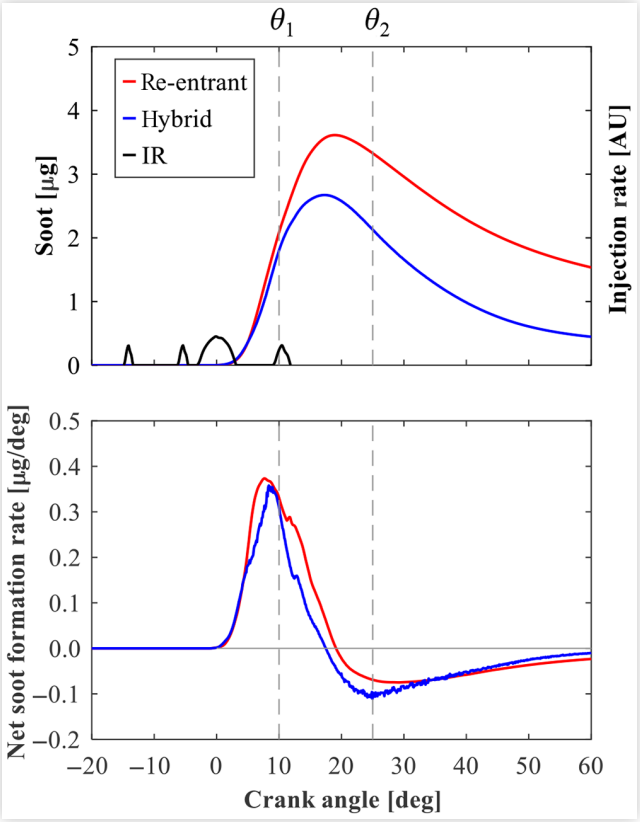

reported in [26]. Moving in the bottom-bump region [Figure 12(c)], the re-entrant bowl shows two merged adjacent flames, remarkably increasing the equivalence ratio in the periphery of the sectors, where higher soot formation is thus expected. Contrarily, the hybrid bowl drives the flame toward the center of the bowl, keeping the flames separated, better utilizing the available oxygen, and avoiding extremely rich regions in the periphery of the sectors.

Once evaluated the equivalence ratio distribution, the effect of the combustion systems on the soot formation and oxidation process was investigated thanks to the detailed PM soot model adopted in the numerical setup. The results in terms of soot mass and net soot formation rate are shown in Figure 13, top and bottom, respectively. After the main EOI, the hybrid bowl shows a reduced net soot formation rate and consequently lower soot mass than with the re-entrant bowl thanks to the minimization of the flame-to-flame interaction and the increment of the air entrainment onto the flame front, enabled by the coupling effect of stepped lip and radial bumps. Moving ahead in the combustion process (from the after EOI to +35 CAD aTDC), when the burn-out of the residual rich pockets is crucial for soot oxidation, the hybrid bowl highlights a higher oxidation rate than the re-entrant bowl.

The hybrid bowl has shown a noticeable reduction of the engine-out soot emissions, and therefore, a deeper investigation on soot mass distribution in the cylinder domain was carried out. Specifically, the computational domain was divided into classes (or bins) accordingly to the soot mass density of each cell and considering the maximum soot density obtained with the re-entrant bowl as a reference. The in-cylinder mass with a soot density between 20% and 40% of the maximum value (Bin #1) was considered as representative of a low-soot density class, while the mass within 60-80% of the maximum soot density value (Bin #2) was selected to represent the high-soot

FIGURE 14 Bin #1 (blue) and Bin #2 (red) soot density iso-surfaces. Left: re-entrant; right: hybrid. WP1: 1500 RPM × 5.0 bar BMEP.

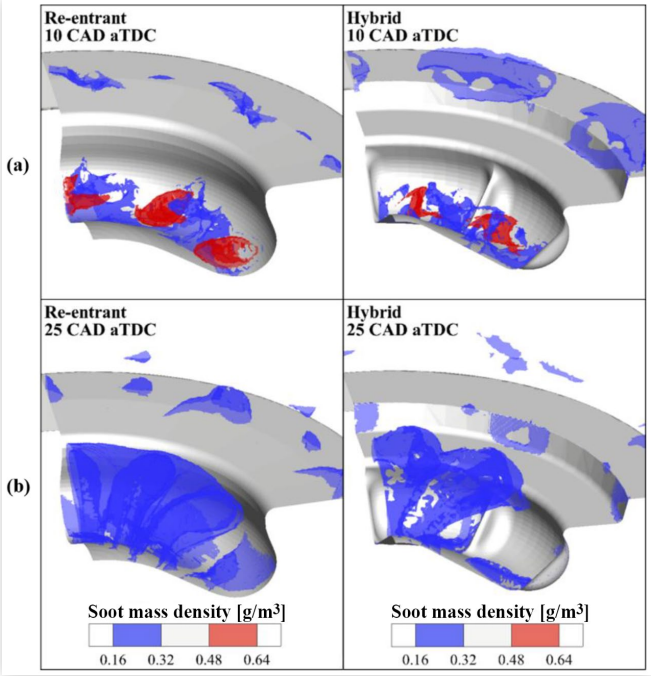

density class. Figure 14 shows Bin #1 (blue) and Bin #2 (red) soot density iso-surfaces during the combustion process for both the combustion systems under investigation, at two different crank angles, $\theta_1$and θ_2, highlighted in Figure 13. At $\theta = \theta_1$, after the main EOI [Figure 14(a)], the re-entrant bowl shows a larger red zone into the periphery of the sectors due to the flame-to-flame interaction previously discussed. On the contrary, the radial bumps on the hybrid bowl mitigate the flames collision, and a lower soot density can be observed in the periphery of the sectors, providing instead the highest soot content in the region between two consecutive bumps. Moreover, the fuel split on the step promotes the combustion in the squish region, thus highlighting a cloud of low-soot density. Late in the cycle, at $\theta = \theta_2$, both the combustion systems have oxidized the high-soot density mass, as highlighted in Figure 14(b); however, the re-entrant bowl still shows higher soot mass within the bowl in comparison with the hybrid design. In fact, on one side, the radial bumps coupled with a reduced SR leads to higher flame recirculation toward the piston dome where available oxygen is present; on the other side, the higher bowl curvature drives the flame toward the cylinder head, creating a more intense tumbling vortex that enhances the mixing into the flame front and thereby the soot oxidation. In addition, the soot mass above the step previously underlined results fully oxidized.

Once the different soot evolutions and their distribution in the combustion systems under investigation were assessed, an EGR rate sweep was performed to assess the EGR tolerance over the well-known soot-$BSNO_x$ and BSFC-$BSNO_x$ trade-offs. From the simulation setup point of view, the EGR rate was modified by varying the gas species fraction within the combustion chamber at IVC, thus considering only the thermal and dilution effects of EGR, keeping the constant volumetric efficiency. In addition, the injection strategy (i.e., energizing and dwell times, rail pressure) was kept constant and equal to the baseline calibration over the EGR sweep. Figure 15 shows the soot-$BSNO_x$ (top) and BSFC-$BSNO_x$ (bottom) trade-offs normalized with respect to the baseline configuration (i.e., re-entrant bowl, nominal EGR rate). It is worth underlining the noticeable soot reduction achieved by the hybrid bowl in comparison with the re-entrant design, highlighting the desirable flatness in the trade-off that allows the NO_x control through EGR without any soot penalty. At constant $BSNO_x$ equal to the baseline value, the hybrid bowl achieves a 70% soot reduction than with the re-entrant bowl, confirming the high potential of the synergy between the stepped lip and the radial bumps for soot mitigation. As far as the BSFC-$BSNO_x$ trade-off is concerned (Figure 15, bottom), similar trends can be highlighted between the analyzed combustion systems. The hybrid bowl leads to a slight BSFC reduction (less than 1% under the nominal EGR rate), but the results become more interesting at a high EGR rate. The improved mixing process, enabled by the combination of stepped lip and radial bumps, allows an EGR increment to keep NO_x under control, with a negligible BSFC worsening (<+1%).

Partial-Load Engine Operating Condition (WP2) The potential benefits in terms of air/fuel mixing enhancement and emission formation mitigation provided by the hybrid bowl were also investigated at 2000 RPM × 8.0 bar BMEP (WP2 in Table 2). As already done for the other engine operating conditions, the results in terms of HRR for each piston bowl are shown in Figure 16. At the Start of Combustion, the re-entrant design shows a more intense pilot combustion, thanks to the higher swirling flow in comparison with the hybrid bowl that allows an enhanced air/fuel mixing in the free spray development. However, near the main event EOI, when the flame-wall interaction phenomena become more important, the hybrid bowl highlights a higher heat release, and the difference between the piston bowls is even more evident than for WP1 due to the increased injected mass.

The equivalence ratio distribution at WP2 on the selected three cutting planes has shown similar behavior than for WP1. Also considering higher load operating conditions, with the hybrid bowl, a reduced flame-to-flame interaction was

FIGURE 15 EGR sweep: normalized trade-offs with respect to the baseline configuration. Top: soot-BSNO$_x$ trade-off; bottom: BSFC-BSNO$_x$ trade-off. WP1: 1500 RPM × 5.0 bar BMEP.

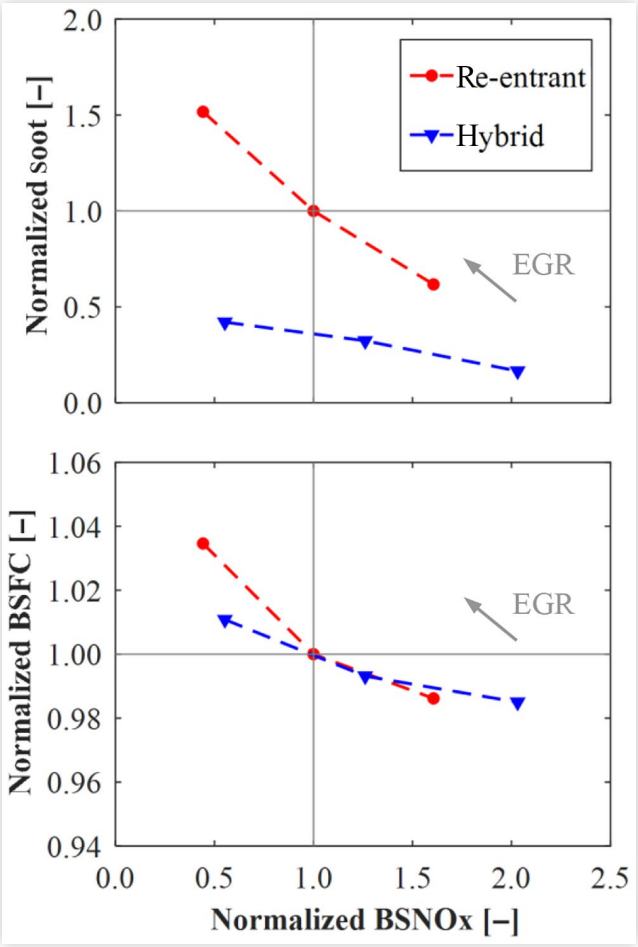

FIGURE 16 HRR and injection rate profile. WP2: 2000 RPM × 8.0 bar BMEP.

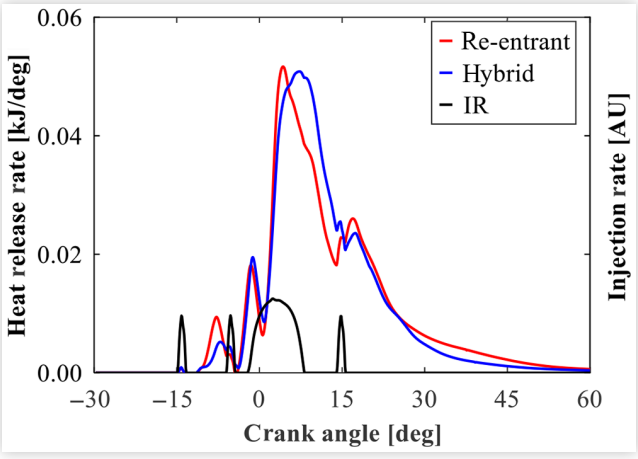

observed, while a more advanced flame propagation toward the bowl center was highlighted due to the more intense tumbling vortex. For the sake of brevity, the equivalence ratio distribution is not reported here.

However, the retarded injection timing and the higher after injection mass in comparison with WP1 could affect the soot oxidation process; therefore, a deeper investigation on soot evolution was carried out. Figure 17 shows the soot mass and net soot formation rate for each combustion system under investigation. After the main EOI, the hybrid bowl highlights a lower soot due to the reduced net soot formation rate. Nevertheless, the soot attenuation with respect to the WP1 is reduced since the higher injected mass for the main event after TDC results in a higher fuel concentration above the step, where a higher soot mass is expected. Moving ahead in the cycle, from +15 CAD to +30 CAD aTDC, the soot oxidation process is significantly affected by the after-injection burn-out, and a different behavior can be highlighted among the combustion systems under investigation. The re-entrant bowl shows a continuous reduction in the net soot formation rate, as depicted in Figure 17, bottom. Contrarily, the hybrid bowl shows a "two-phase" trend in the net soot formation rate. Firstly, a stable phase can be observed since the soot oxidation is slowed down by the higher soot formation due to the after-injection burn-out. However, at this stage the hybrid bowl still shows a lower net soot formation rate than with the re-entrant bowl, thus confirming the efficacy of the proposed design. After that, the net soot formation rate of the hybrid bowl decreases, reaching a similar value to the re-entrant bowl.

More details concerning the in-cylinder soot formation can be highlighted by evaluating the soot density distribution, following the same methodology described for WP1. Figure 18 shows low-soot density (Bin #1, blue) and high-soot density (Bin #2, red) classes iso-surfaces at two different crank angles, $\theta_1$and θ_2, highlighted in Figure 17. As already shown for WP1, at $\theta = \theta_1$ after the main EOI [Figure 18(a)], the re-entrant bowl shows a more intense high-soot density content in the periphery of the sectors due to the flame-to-flame interaction. On the contrary, two different high-soot density regions can be highlighted for the hybrid bowl: on one side, the enhanced tumbling vortex directs the rich fuel region toward the piston center, reducing the net soot formation rate (see Figure 17, bottom) thanks to the higher air entrainment. On the other side, the fuel split on the step pushes fuel in the squish region increasing the soot formation, and this effect is even more evident than WP1 due to the higher injected mass after TDC. During the after-injection burn-out, at $\theta = \theta_2$, the combustion systems show a different behavior [Figure 18(b)]. In the re-entrant bowl, the after-injection impinges on the piston bowl rim, limiting the propagation in the squish region, and high soot formation is highlighted in the jet periphery, as shown within the black dashed circles. For the hybrid bowl, the more intense recirculating flow toward the cylinder center strongly interacts with the after-injection spray core. This flame's

FIGURE 17 Soot PM model results. Top: in-cylinder soot mass; bottom: net formation rate of in-cylinder soot mass. WP2: 2000 RPM × 8.0 bar BMEP.

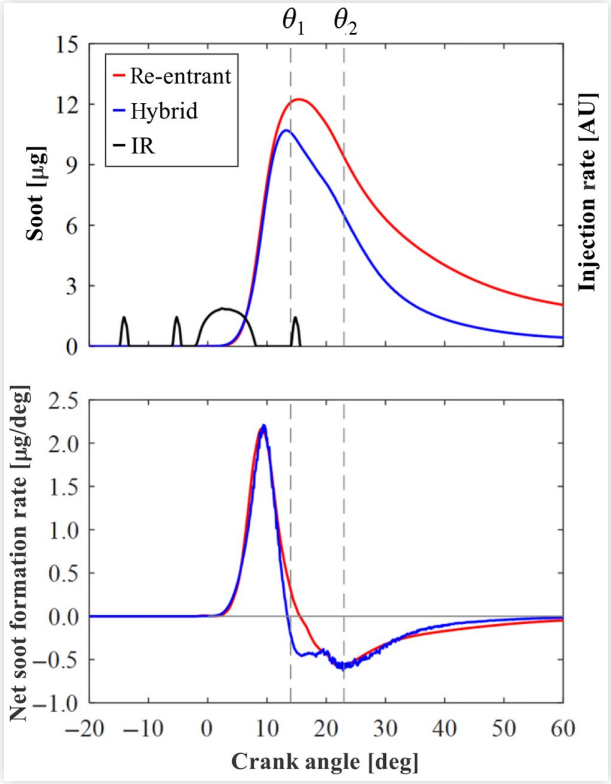

FIGURE 18 Bin #1 (blue) and Bin #2 (red) soot density iso-surfaces. Left: re-entrant; right: hybrid. WP2: 2000 RPM × 8.0 bar BMEP.

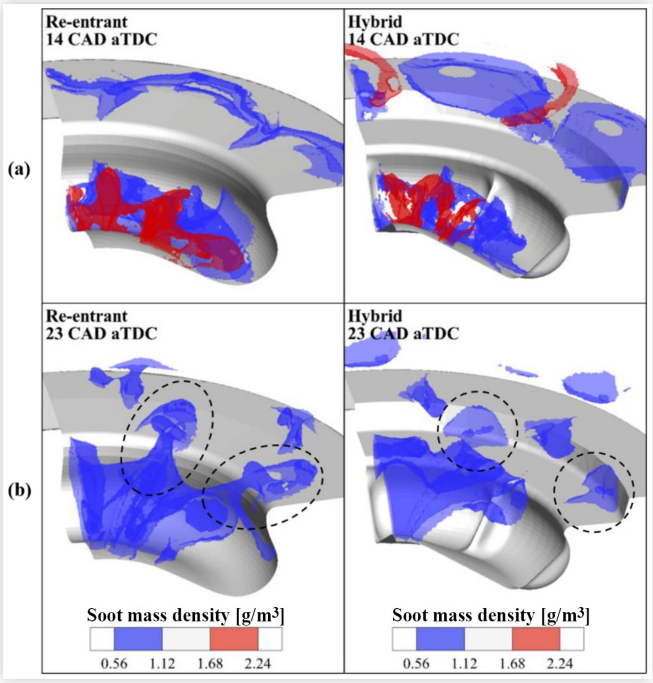

interaction increases the rich mass and thus the soot formation, resulting in the stable phase of the net soot formation rate previously assessed (see Figure 17, bottom). Nevertheless, the after-injection propagates and burns above the step (as highlighted by the black dashed circles), enhancing the local temperature distribution and, thus, being helpful for the oxidation of the high-soot density region previously highlighted.

Figure 19 shows the typical soot-BSNO$_x$ and BSFC-BSNO$_x$ trade-offs curves for the EGR sweep at WP2, normalized with respect to the baseline configuration (i.e., re-entrant bowl, nominal EGR rate). As for WP1, the hybrid bowl shows a remarkable improvement of soot-BSNO$_x$ trade-off, with a soot reduction of 70% at baseline BSNO$_x$ level, linked to a slight BSFC improvement (−1%). The assessment at WP2 confirms the potential benefits of this innovative hybrid bowl for soot mitigation, already highlighted at rated power (WP3) and partial-load (WP1) engine operating conditions.

4. Conclusions

This work aims to assess through numerical simulations, the effects on the combustion process of an innovative AM-enabled piston bowl, named "hybrid," featuring both a highly-reentrant sharp-stepped bowl and a number of radial bumps in the inner bowl rim equal to the injector nozzle holes. This innovative hybrid bowl was designed for a light-duty diesel engine and was compared with a conventional re-entrant bowl, under different engine operating conditions. Firstly, for the hybrid bowl, the spray targeting optimization was carried out over different injector protrusions and two SR levels. Once the optimal combination of spray targeting and swirling flow was assessed, the combustion analysis was carried out for three engine operating conditions: one at rated power and two at partial load. In this way, the impact of the combustion systems on the near-wall flame evolution and the soot formation/oxidation process was assessed. The main findings of this work can be summarized as follow:

- The hybrid design highlighted high sensitivity to the injector protrusion both in terms of soot and BSFC, suggesting that the fuel split on the step is a crucial aspect for the optimization of the spray targeting. The optimal results were obtained for the nominal injector protrusion, thanks to which a more evenly distributed fuel mass above the step and within the bowl is obtained. With this injector protrusion, both soot and BSFC were significantly reduced in comparison with the re-entrant bowl (−40% and −2%, respectively). Also considering a reduced SR, the nominal injector protrusion still showed the best results. Nevertheless, the nominal SR was required to keep a lower soot and BSFC than with the re-entrant bowl due to the enhanced mixing process.

FIGURE 19 EGR sweep: normalized trade-offs with respect to the baseline configuration. Top: soot-BSNO$_x$ trade-off; bottom: BSFC-BSNO$_x$ trade-off. WP2: 2000 RPM × 8.0 bar BMEP.

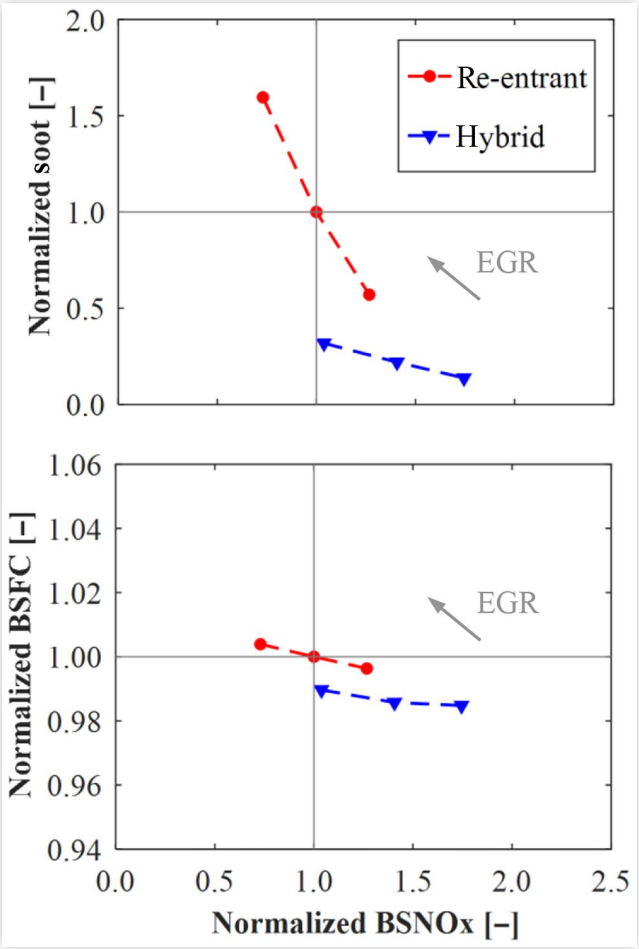

- Considering the optimal calibration (nominal injector protrusion, nominal SR), the combustion analysis was carried out for all three engine operating conditions under investigation. At full load, the innovative hybrid bowl showed a higher HRR during the mixing-controlled combustion phase due to the reduced flame-to-flame interaction enabled by the radial bumps.
- At partial load, the hybrid bowl has shown a strong impact on equivalence ratio distribution, avoiding the formation of rich regions near the bowl surface thanks to the minimized flames collision. This resulted in lower soot formation after the end of injection of the main event. Moreover, the more intense tumbling vortex in the hybrid design led to a higher soot oxidation rate in the late combustion phase.
- At partial load, the innovative hybrid concept has shown an impressive improvement of soot-NO$_x$ trade-off over an EGR sweep. At baseline NO$_x$, a 70% soot reduction in comparison with the re-entrant bowl was achieved. Considering the BSFC-NO$_x$ trade-off, no significant differences were observed in comparison with the re-entrant bowl, providing up to 1% BSFC reduction. The desired flatness in the trade-off allowed a higher EGR rate for NO$_x$ mitigation without any soot penalties and any detrimental effect on fuel consumption.

Contact Information

Prof. Federico Millo
Politecnico di Torino - Energy Department
C.so Duca degli Abruzzi
10129 Torino
ITALY
federico.millo@polito.it

Abbreviations

AM - Additive Manufacturing
AMR - Adaptive Mesh Refinement
BMEP - Brake Mean Effective Pressure
BSFC - Brake-Specific Fuel Consumption
BSNO$_x$ - Brake-Specific NO$_x$
CAD aTDC - Crank Angle Degrees after Top Dead Center
CFD - Computational Fluid Dynamics
CIV - Combustion Image Velocimetry
EGR - Exhaust Gas Recirculation
EOI - End of Injection
HRR - Heat Release Rate
IVC - Intake Valve Closure
KH-RT - Kelvin Helmholtz and Rayleigh Taylor
NTC - No Time Counter
PAH - Polycyclic Aromatic Hydrocarbons
PM - Particulate Mimic
RANS - Reynolds-averaged Navier-Stokes
RMZ - Radial Mixing Zone
RNG - Renormalization Group
SCE - Single-Cylinder Engine
SCR - Selective Catalytic Reduction
SR - Swirl Ratio
TDC - Top Dead Center
VGT - Variable Geometry Turbine
WP - Working Point

References

1. Belgiorno, G., Dimitrakopoulos, N., Di Blasio, G., Beatrice, C. et al., "Effect of the Engine Calibration Parameters on Gasoline Partially Premixed Combustion Performance and Emissions Compared to Conventional Diesel Combustion in

a Light-Duty Euro 6 Engine," *Applied Energy* 228 (2018): 2221-2234, https://doi.org/10.1016/j.apenergy.2018.07.098.

2. Benajes, J., García, A., Monsalve-Serrano, J., and Lago Sari, R., "Fuel Consumption and Engine-Out Emissions Estimations of a Light-Duty Engine Running in Dual-Mode RCCI/CDC with Different Fuels and Driving Cycles," *Energy* 157 (2018): 19-30, https://doi.org/10.1016/j.energy.2018.05.144.
3. Pastor, J.V., García, A., Micó, C., and Lewiski, F., "An Optical Investigation of Fischer-Tropsch Diesel and Oxymethylene Dimethyl Ether Impact on Combustion Process for CI Engines," *Applied Energy* 260 (2020): 114238, https://doi.org/10.1016/j.apenergy.2019.114238.
4. Zhang, T., Eismark, J., Munch, K., and Denbratt, I., "Effects of a Wave-Shaped Piston Bowl Geometry on the Performance of Heavy Duty Diesel Engines Fueled with Alcohols and Biodiesel Blends," *Renewable Energy* 148 (2020): 512-522, https://doi.org/10.1016/j.renene.2019.10.057.
5. Lückert, P., Arndt, S., Duvinage, F., Kemmner, M. et al., "The New Mercedes-Benz 4-Cylinder Diesel Engine OM654 - The Innovative Base Engine of the New Diesel Generation," in *24th Aachen Colloquium Automobile and Engine Technology*, Aachen, 867-892, 2015.
6. ICCT, "Shifting Gears: The Effects of a Future Decline in Diesel Market Share on Tailpipe CO2 and NOX Emissions in Europe," 2017, https://theicct.org/sites/default/files/publications/Shifting-gears-EU%20diesel-futures_ICCT-white-paper_06072017_vF.pdf.
7. Sanchez, F.P., Bandivadekar, A., and German, J., "Estimated Cost of Emission Reduction Technologies for LDVs," International Council on Clean Transportation, 1-136, March, 2012.
8. ICCT, "Costs of Emission Reduction Technologies for Diesel Engines Used in Non-Road Vehicles and Equipment," 2018, https://theicct.org/sites/default/files/publications/Non_Road_Emission_Control_20180711.pdf.
9. Miles, P.C. and Andersson, Ö., "A Review of Design Considerations for Light-Duty Diesel Combustion Systems," *International Journal of Engine Research* 17, no. 1 (2016): 6-15, https://doi.org/10.1177/1468087415604754.
10. Leach, F., Ismail, R., Davy, M., Weall, A. et al., "The Effect of a Stepped Lip Piston Design on Performance and Emissions from a High-Speed Diesel Engine," *Applied Energy* 215 (2018): 679-689, https://doi.org/10.1016/j.apenergy.2018.02.076.
11. Busch, S., Zha, K., Perini, F., Reitz, R. et al., "Bowl Geometry Effects on Turbulent Flow Structure in a Direct Injection Diesel Engine," SAE Technical Paper 2018-01-1794, 2018, https://doi.org/10.4271/2018-01-1794.
12. Millo, F., Piano, A., Peiretti Paradisi, B., Boccardo, G. et al., "The Effect of Post Injection Coupled with Extremely High Injection Pressure on Combustion Process and Emission Formation in an Off-Road Diesel Engine: A Numerical and Experimental Investigation," SAE Technical Paper 2019-24-0092, 2019, https://doi.org/10.4271/2019-24-0092.
13. Cornwell, R. and Conicella, F., Direct injection diesel engines. U.S. Patent 8770168 B2, Ricardo UK Limited, West Sussex (GB), 2014.
14. Smith, A., "Ricardo Low Emissions Combustion Technology Helps JCB Create the Off-Highway Industry's Cleanest Engine," Ricardo Press Release, 2010, https://ricardo.com/news-and-media/news-and-press/ricardo-low-emissions-combustion-technology-helps, accessed September 2021.
15. Eder, T., Kemmner, M., Lückert, P., and Sass, H., "OM 654—Launch of a New Engine Family by Mercedes-Benz," *MTZ Worldwide* 77, no. 3 (2016): 60-67.
16. Zha, K., Busch, S., Warey, A., Peterson, R. et al., "A Study of Piston Geometry Effects on Late-Stage Combustion in a Light-Duty Optical Diesel Engine Using Combustion Image Velocimetry," *SAE Int. J. Engines* 11, no. 6 (2018): 783-804, https://doi.org/10.4271/2018-01-0230.
17. Busch, S., Zha, K., Kurtz, E., Warey, A. et al., "Experimental and Numerical Studies of Bowl Geometry Impacts on Thermal Efficiency in a Light-Duty Diesel Engine," SAE Technical Paper 2018-01-0228, 2018, https://doi.org/10.4271/2018-01-0228.
18. Styron, J., Baldwin, B., Fulton, B., Ives, D. et al., "Ford 2011 6.7L Power Stroke® Diesel Engine Combustion System Development," SAE Technical Paper 2011-01-0415, 2011, https://doi.org/10.4271/2011-01-0415.
19. Yoo, D., Kim, D., Jung, W., Kim, N. et al., "Optimization of Diesel Combustion System for Reducing PM to Meet Tier4-Final Emission Regulation without Diesel Particulate Filter," SAE Technical Paper 2013-01-2538, 2013, https://doi.org/10.4271/2013-01-2538.
20. Perini, F., Busch, S., Zha, K., Reitz, R. et al., "Piston Bowl Geometry Effects on Combustion Development in a High-Speed Light-Duty Diesel Engine," SAE Technical Paper 2019-24-0167, 2019, https://doi.org/10.4271/2019-24-0167.
21. Andersson, Ö. and Miles, P.C., "Diesel and Diesel LTC Combustion," *Encyclopedia of Automotive Engineering* (Hoboken: Wiley, 2014), 1-36, https://doi.org/10.1002/9781118354179.auto120.
22. Eismark, J., Balthasar, M., Karlsson, A., Benham, T. et al., "Role of Late Soot Oxidation for Low Emission Combustion in a Diffusion-controlled, High-EGR, Heavy Duty Diesel Engine," SAE Technical Paper 2009-01-2813, 2009, https://doi.org/10.4271/2009-01-2813.
23. Eismark, J. and Balthasar, M., Device for reducing emissions in a vehicle combustion engine. U.S. Patent 8499735B2, Volvo Lastvagnar AB, Göteborg (SE), 2013.
24. Eismark, J., Andersson, M., Christensen, M., Karlsson, A. et al., "Role of Piston Bowl Shape to Enhance Late-Cycle Soot Oxidation in Low-Swirl Diesel Combustion," *SAE Int. J. Engines* 12, no. 3 (2019): 233-249, https://doi.org/10.4271/03-12-03-0017.
25. Eismark, J., Christensen, M., Andersson, M., Karlsson, A. et al., "Role of Fuel Properties and Piston Shape in Influencing Soot Oxidation in Heavy-Duty Low Swirl Diesel Engine Combustion," *Fuel* 254 (2019): 115568, https://doi.org/10.1016/j.fuel.2019.05.151.

26. Millo, F., Piano, A., Roggio, S., Bianco, A. et al., "Numerical Investigation on Mixture Formation and Combustion Process of Innovative Piston Bowl Geometries in a Swirl-Supported Light-Duty Diesel Engine," *SAE Int. J. Engines* 14, no. 2 (2021): 247-262, https://doi.org/10.4271/03-14-02-0015.
27. Dolan, R., Budde, R., Schramm, C., and Rezaei, R., "3D Printed Piston for Heavy-Duty Diesel Engines," in *2018 NDIA Ground Vehicle Systems Engineering and Technology Symposium Power & Mobility (P&M) Technical Session*, Novi, MI, August 7-9, 2018, https://events.esd.org/wp-content/uploads/2018/07/3D-Printed-Piston-for-Heavy-Duty-Diesel-Engines.pdf.
28. Belgiorno, G., Boscolo, A., Dileo, G., Numidi, F. et al., "Experimental Study of Additive-Manufacturing-Enabled Innovative Diesel Combustion Bowl Features for Achieving Ultra-Low Emissions and High Efficiency," *SAE Int. J. Adv. & Curr. Prac. in Mobility* 3, no. 1 (2021): 672-684, https://doi.org/10.4271/2020-37-0003.
29. Pastor, J.V., García, A., Micó, C., Lewiski, F. et al., "Effect of a Novel Piston Geometry on the Combustion Process of a Light-Duty Compression Ignition Engine: An Optical Analysis," *Energy* 221 (2021): 119764, https://doi.org/10.1016/j.energy.2021.119764.
30. Pastor, J.V., García, A., Micó, C., and Lewiski, F., "Soot Reduction for Cleaner Compression Ignition Engines through Innovative Bowl Templates," *International Journal of Engine Research* 22, no. 8 (2020): 2477-2491, https://doi.org/10.1177/1468087420951324.
31. Millo, F., Piano, A., Peiretti Paradisi, B., Marzano, M.R. et al., "Development and Assessment of an Integrated 1D-3D CFD Codes Coupling Methodology for Diesel Engine Combustion Simulation and Optimization," *Energies* 13 (2020): 1612, https://doi.org/10.3390/en13071612.
32. Piano, A., Millo, F., Boccardo, G., Rafigh, M. et al., "Assessment of the Predictive Capabilities of a Combustion Model for a Modern Common Rail Automotive Diesel Engine," SAE Technical Paper 2016-01-0547, 2016, https://doi.org/10.4271/2016-01-0547.
33. Piano, A., Millo, F., Postrioti, L., Biscontini, G. et al., "Numerical and Experimental Assessment of a Solenoid Common-Rail Injector Operation with Advanced Injection Strategies," *SAE Int. J. Engines* 9, no. 1 (2016): 565-575, https://doi.org/10.4271/2016-01-0563.
34. Piano, A., Boccardo, G., Millo, F., Cavicchi, A. et al., "Experimental and Numerical Assessment of Multi-Event Injection Strategies in a Solenoid Common-Rail Injector," *SAE Int. J. Engines* 10, no. 4 (2017): 2129-2140, https://doi.org/10.4271/2017-24-0012.
35. Richards, K.J., Senecal, P.K., and Pomraning, E., "Converge 2.3 Manual," Convergent Science Inc., Madison, WI, 2016.
36. Issa, R.I., "Solution of the implicitly discretised fluid flow equations by operator-splitting," *Journal of Computational Physics* 62, no. 1 (1986): 40-65, https://doi.org/10.1016/0021-9991(86)90099-9.
37. Rhie, C.M. and Chow, W.L., "Numerical study of the turbulent flow past an airfoil with trailing edge separation," *AIAA Journal* 21, no. 11 (1983): 1525-1532, https://doi.org/10.2514/3.8284.
38. Orszag, S.A., Yakhot, V., Flannery, W.S., Boysan, F. et al., "Renormalization Group Modeling and Turbulence Simulations," *Near-Wall Turbulent Flows* 13, (1993): 1031-1046.
39. Yakhot, V., Orszag, S.A., Thangam, S., and Gatski, TB., "Development of turbulence models for shear flows by a double expansion technique," *Physics of Fluids A: Fluid Dynamics* 4, (1992): 1510, https://doi.org/10.1063/1.858424.
40. Versteeg, H.K. and Malalasekera, W., "An Introduction to Computational Fluid Dynamics: The Finite Volume Method," 2007.
41. Amsden, A.A., "KIVA-3V: A Block Structured KIVA Program for Engines with Vertical or Canted Valves," Los Alamos National Laboratory Technical Report LA-13313-MS, 1997.
42. Reitz, R.D. and Bracco, F.V., "Mechanisms of Breakup of Round Liquid Jets," *Encyclopedia of Fluid Mechanism* (Houston: Gulf Pub. Co., Book Division, 1986), Vol. 3, 233-249.
43. Amsden, A.A., O'Rourke, P.J., and Butler, T.D., "KIVA-II: A Computer Program for Chemically Reactive Flows with Sprays," Los Alamos National Laboratory Technical Report LA-11560-MS, 1989.
44. Schmidt, D.P. and Rutland, C.J., "A New Droplet Collision Algorithm," *Journal of Computational Physics* 164, no. 1 (2000): 62-80, https://doi.org/10.1006/jcph.2000.6568.
45. O'Rourke, P. and Amsden, A., "The Tab Method for Numerical Calculation of Spray Droplet Breakup," SAE Technical Paper 872089, 1987, https://doi.org/10.4271/872089.
46. O'Rourke, P. and Amsden, A., "A Spray/Wall Interaction Submodel for the KIVA-3 Wall Film Model," SAE Technical Paper 2000-01-0271, 2000, https://doi.org/10.4271/2000-01-0271.
47. Zeuch, T., Moréac, G., Ahmed, S.S., and Mauss, F., "A Comprehensive Skeletal Mechanism for the Oxidation of n-Heptane Generated by Chemistry-Guided Reduction," *Combustion and Flame* 155, no. 4 (2008): 651-674, https://doi.org/10.1016/j.combustflame.2008.05.007.
48. Frenklach, M. and Wang, H., "Detailed Modeling of Soot Particle Nucleation and Growth," *Symposium (International)*

on Combustion 23, no. 1 (1991): 1559-1566, https://doi.org/10.1016/S0082-0784(06)80426-1.

49. Kazakov, A., Wang, H., and Frenklach, M., "Detailed Modeling of Soot Formation in Laminar Premixed Ethylene Flames at a Pressure of 10 Bar," *Combustion and Flame* 100, no. 1-2 (1995): 111-120, https://doi.org/10.1016/0010-2180(94)00086-8.
50. Kazakov, A. and Frenklach, M., "Dynamic Modeling of Soot Particle Coagulation and Aggregation: Implementation with the Method of Moments and Application to High-Pressure Laminar Premixed Flames," *Combustion and Flame* 114, no. 3-4 (1998): 484-501, https://doi.org/10.1016/S0010-2180(97)00322-2.
51. Dolak, J., Shi, Y., and Reitz, R., "A Computational Investigation of Stepped-Bowl Piston Geometry for a Light Duty Engine Operating at Low Load," SAE Technical Paper 2010-01-1263, 2010, https://doi.org/10.4271/2010-01-1263.